$52.90

GEOLOGICAL SURVEY OF CANADA

OPEN FILE 1800

Pn source-specific station corrections for IMS stations in eastern Asia

K.-Y. Chun, N. Vasiliev, J. Liu

2004

GEOLOGICAL SURVEY OF CANADA

OPEN FILE 1800

Pn Source Specific Station Corrections for IMS stations in Eastern Asia

K.-Y. Chun, N. Vasiliev, J. Liu

2004

Technical Report for Geological Survey of Canada Class Grant: Part B

Pn SOURCE SPECIFIC STATION CORRECTIONS FOR IMS STATIONS IN EASTERN ASIA

Kin-Yip Chun

Nikolai Vasiliev

Jingsong Liu

Seismological Laboratory

Department of Physics

University of Toronto

Toronto, Ontario M5S 2J5

SEMI-ANNUAL TECHNICAL REPORT: 1 March to 31 August 31 2003

Prepared for:

COMPREHENSIVE NUCLEAR TEST BAN TREATY VERIFICATION DIVISION

GEOLOGICAL SURVEY

CANADA

TABLE OF CONTENTS
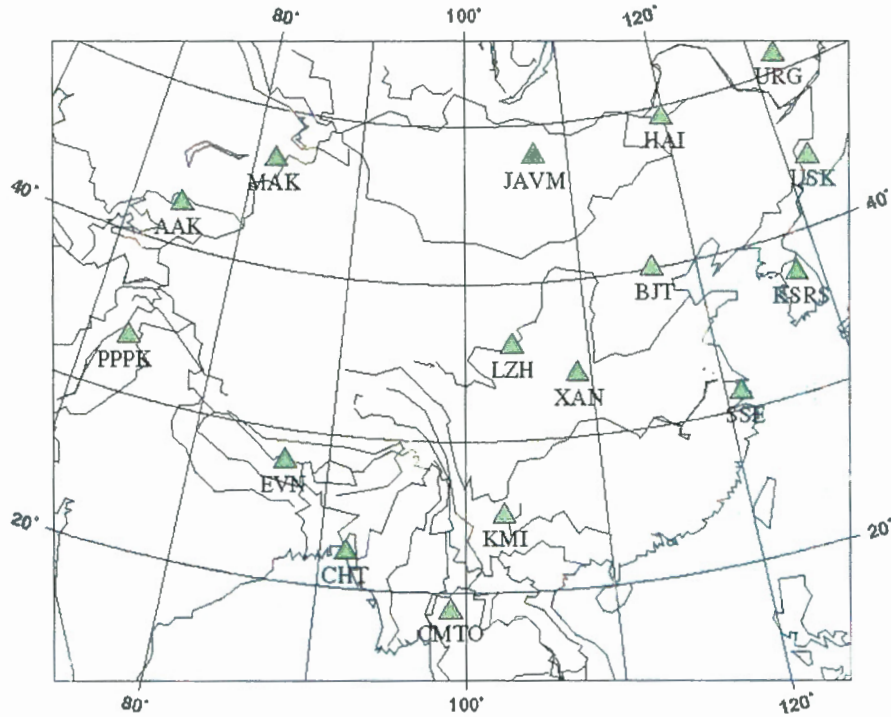
9. 1. INTRODUCTION

In part B of the project we develop Pn SSSCs for 16 International Monitoring System (IMS) stations in Eastern Asia.

Figure 1. IMS seismic stations in area of interest

We use data from the following sources:
- Bulletins of Provincial Seismological Bureaus (PSB) in China.
  Raw Pn arrival-time data were initially compiled at the Institute of Geology and Geophysics, Chinese Academy of Sciences, Beijing, and were later reprocessed at the Seismological Laboratory, University of Toronto;
- Annual Bulletin of Chinese Earthquakes (ABCE);
- Quarterly Earthquake Report of the Beijing Telemetered Seismic Network.
  The quarterly is published by the Institute of Geophysics, China Seismological Bureau (CSB - formerly State Seismological Bureau of China);
- Annual Report (AR)
  The report is published by CSB;
- Center for Monitoring Research (CMR), Arlington, Virginia, U.S.A;
- Japan Meteorological Agency (99);
- Korean Meteorological Administration (4);
- Geophysical Survey of Russia (30);
- Central Weather Bureau (137) (Taiwan, China);
- Kazakhstan (22)*;
- Mongolia (1)#.

Number in parenthesis refers to the number of contributing stations by various agencies in regions adjacent to continental China.

* Some of the 22 stations from Kazakhstan may be temporary deployments.
# The lone Mongolian station is OBM.

AR lists all available phase picks from China and from regions near China that are used in determining the event location and origin time. These phase picks are not confined to any particular provincial seismological bureau network. We use AR when searching initially for GT5 events (ground truth events with location error estimated to be less than 5 km).

The time spans for our main data sources are as follows:

1978	1984	1995	1999
PSB			
Unknown	AR		
Not covered	ABCE		

The project consists of three main steps:

- Preliminary analysis, screening and processing of Pn travel-time data;
- Development of Pn velocity model and the model describing the crustal portion of the Pn travel time;
- Development and validation of SSSCs.

The Pn ray coverage in China, owing to a higher station density and active seismicity, is much denser than that in Canada (Part A of this GSC Class Grant). We opt for a more sophisticated Pn tomographic inversion method here (than in Part A) in order to achieve optimal results. The main distinguishing features of the new approach are:

- The algorithm is more flexible. It allows us to produce a Pn velocity map showing greater details (higher spatial resolution).
- The Pn velocity inversion produces, as byproducts, the so-called station and event delays. The former pertains to the travel time between the base of the crust and a given station and the latter between a given hypocentre and the base of the crust. Both the station and event delays are a function of the local crustal velocity and thickness.
- We make use of the station and event delays to produce a crustal delay map for the study region, thus removing the need for *ad hoc*, predefined crust velocity models such as those used in Part A of our Pn SSSC study in Canada.

Validation tests are carried out using the GT5 events described below. Even with very good station coverage, there is no absolute guarantee that our selected AR locations are true GT5 events. Brief description of *sgap* criteria can be found in "Validation" (section 6 of the report for Part A).

2. DATA

The China Seismological Bureau (CSB) constitutes our principal source of data. ABCE bulletin, published by CSB, is China's official medium for international seismic data exchange. Our Pn selection criteria are described below. While they publish nearly identical event locations, AR provides information on many more phase picks than does ABCE, and is therefore our preferred reference source for Pn arrival-time data. The AR data in the period 1995-1999 alone contain 135,620 P/Pn arrivals. When data from all sources are added up (1978-1999) - care being taken to remove any multiply reported events - the final number rises to 228,259 P/Pn arrivals. Ours represents the first comprehensive Pn database ever assembled to date from China's national seismic network. For the period 1978-1999 we record 21,217 events and 1,139 stations.

Low-magnitude earthquakes not reported by AR/ABCE are found in PSB bulletins. The PSB bulletins report epicentral locations computed using only their individual provincial network data, giving rise to multiple reporting of the same event by several adjacent provincial networks. Our Chinese colleagues are credited with manually transferring the arrival-time entries one by one from PSB paper bulletins into their computer database while keeping track of multiple event listings to avoid data redundancy. Several person-months of our effort were expended reviewing, correcting, and selecting from, the voluminous data initially processed in China.

Between 1978 and 1999 seismic phases reported by PSBs amount to 2,798,802 arrivals of mostly short-distance crustal phases from 77,972 events. These data would suggest exceptionally high accuracy of the Chinese epicentral solutions [e.g., Hearn et al., 2003] – a reassuring piece of information to be had. The high-accuracy location solutions allow us to identify events that meet GT5 (ground truth events with an estimated location error not exceeding 5 km) criteria, as proposed by Bondar [2002]. Applying these criteria to our Chinese data, we found 6,492 potentially qualifying events.

Not every potential GT5 event produced good-quality Pn recordings in the AR bulletin. Of the above 6,492 events, we found 278 earthquakes in our database, each of which satisfies the following two additional criteria: 1) it produced adequate number of Pn recordings for us to conduct a meaningful validation test; and 2) it is an "open" event in the sense that it is cross-listed in ABCE. As we stated before, while the AR and ABCE epicentral solutions are practically identical, nearly all phase pickings from various PSB monthly bulletins appear in Annual Report but only a small fraction of them appear in ABCE bulletin. We exclude Pn travel times produced by the validation (278) events from the data actually used for tomographic inversion in order to have them qualify as independent data.

The map below displays the event distribution.
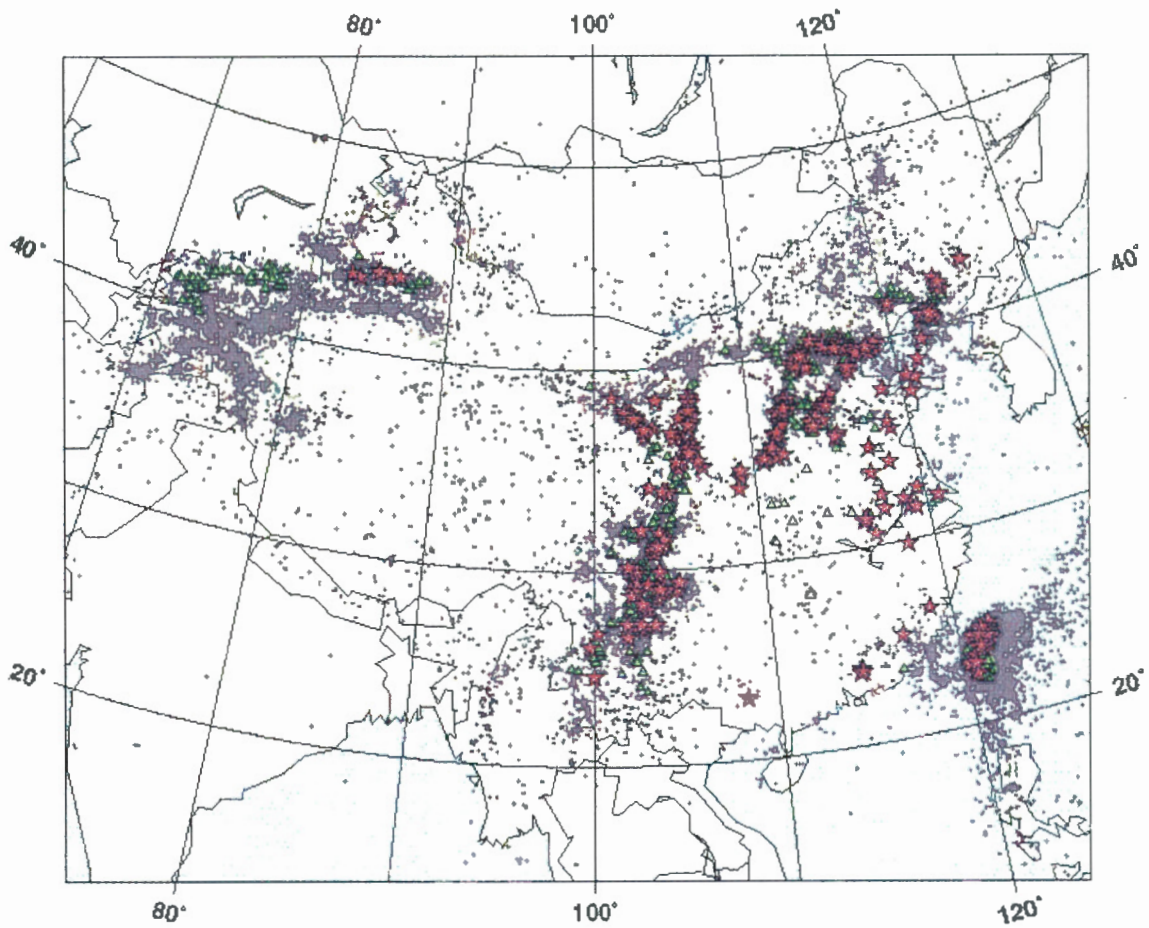
Figure 2. Event distribution:
All events used in Pn tomography (21,217) – points
All GT5 events (6,492) – triangles
GT5 events from AR/ABCE – stars

The selection criteria are as follows for Pn arrival times for the tomographic inversion:

- **Epicentral distance range**: $1.9^0 - 14.1^0$
- **Phases**: Recent (1995-1999) PSB monthly bulletins, being the most reliable source of phase picks, are first analyzed to delineate the Pn travel-time characteristics, especially at short distances, to help weed out Pg arrivals incorrectly identified as Pn. For older PSB bulletins (1978-1994) only Pn within epicentral distances $3.6^0 - 14.1^0$ are accepted for processing to avoid phase picks marked Pn, which may have been Pg in disguise (i.e., Pg mislabeled as Pn).
- **Phase picking quality**: The bulk of our data have come from China rather than from its neighbouring regions. The Chinese seismographs vary from province to province. The output medium ranges from photographic paper to digital storage devices. The provincial seismological bureaus use different training manuals for the analysts who pick arrival times. One constant is the phase picking accuracy: it is stringent throughout China. The picking error in most cases is about 0.3s or better.

- **Event location and origin time**: We accept, where available, epicentral determinations listed in Annual Report. The AR epicentral solutions are based on available phase arrival times from all recording stations in China plus some from stations near China.
- For low-magnitude events not reported by the AR/ABCE bulletins, we rely on the PSB monthly bulletin.
- We use only those events whose estimated focal depth is less than 42 km to weed out mantle earthquakes.

Residuals from average travel time: we apply a relaxed criterion when weeding out the outliers. At any given epicentral distance, we allow a maximum departure from the average Pn travel time to be ± 10 sec. Given the extreme variation in crustal thickness and Pn velocity across East Asia, we apply this wide window to ensure that all Pn signals will be included – at the risk of inadvertently accepting some wrong phases. We note that some outliers define linear trends located one minute or one hour distant from the average Pn arrivals. They are obviously due to misreading of the clock time. These errors are corrected first - prior to the application of the ± 10 sec window.
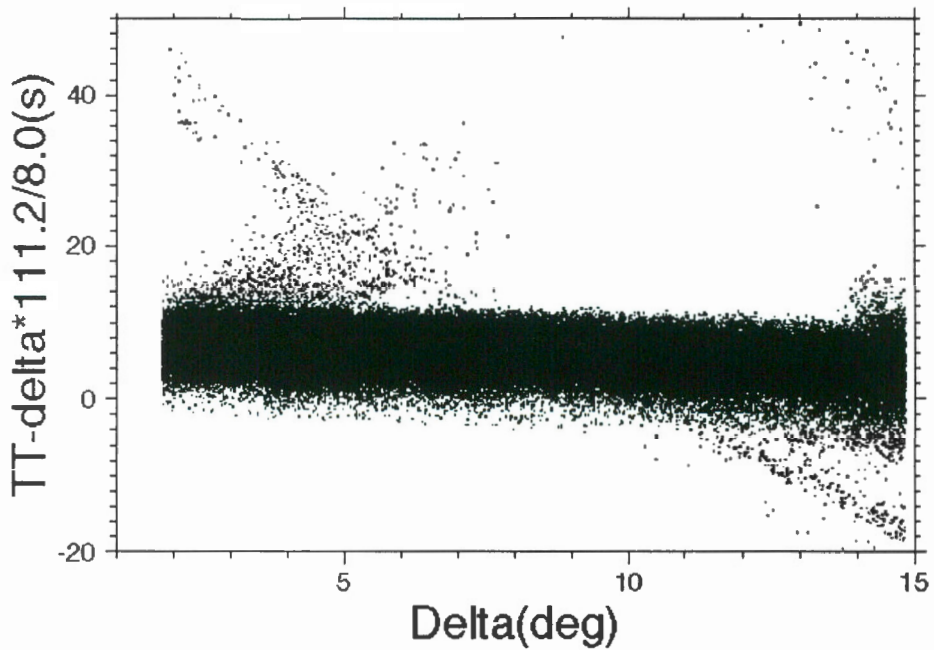

Figure 3. Reduced Pn travel times

Figure 3 shows the pre-screening reduced travel times. The screening criteria are described in the text. Some outliers are wrongly identified Pg phases; some (seen at short distances) are reflected P phases. Refracted P signals propagate at apparent velocities that are much higher than are expected of Pn (beyond 11^0).

Figures 4 below shows epicentral distribution of all Pn data prior to the application of the screening criteria; Figure 5 illustrates the Pn ray coverage after screening; and Figure 6 displays the epicentral locations (red) and stations (blue) used in this study, respectively.
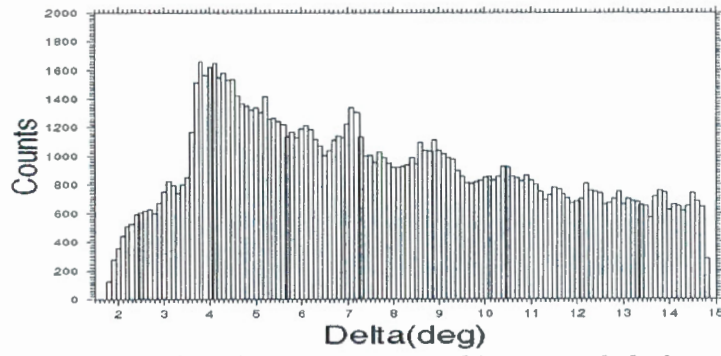
Figure 4. *Epicentral distribution of potential Pn arrivals before screening*
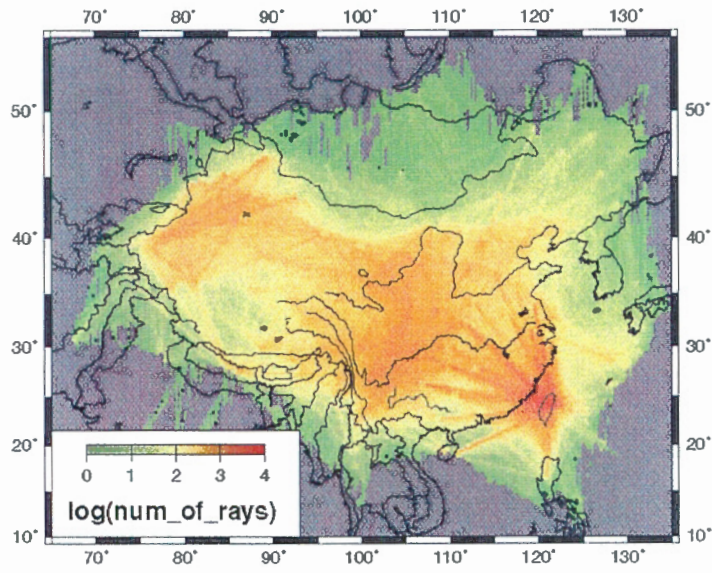
Figure 5. *Pn Ray coverage after screening*
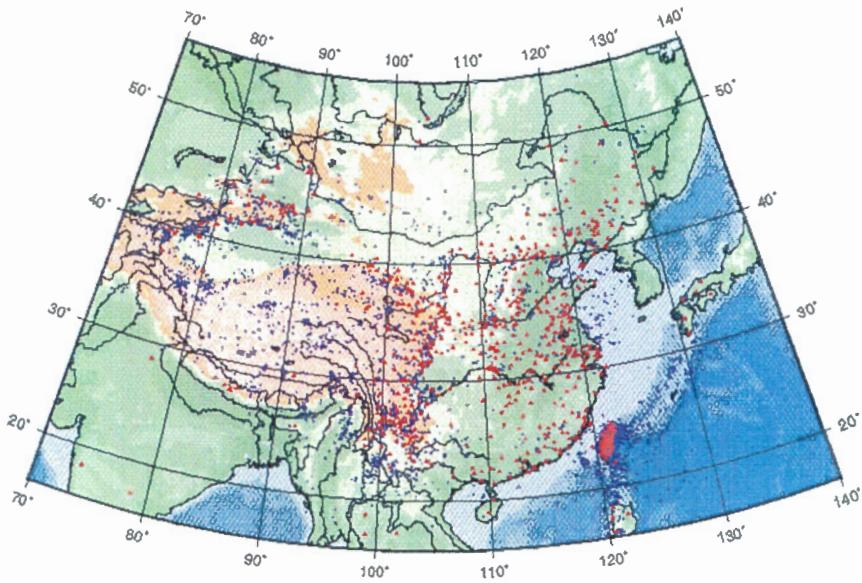
Figure 6. *Stations (red) and events (blue) used in this study*

3. CRUSTAL AND MANTLE MODELS

As in Part A, we carry out a travel-time tomography assuming that the head-wave model applies to Pn ($\Delta = 1.9^0 - 14.1^0$). Taking advantage of the superior data density in China to yield high-resolution images of the uppermost mantle, we adopt the method of Hearn [1996] in which Pn travel time along a given path is described as the sum of an average (or characteristic) station delay a, an event delay b, and the cumulative travel time across the uppermost-mantle cells, the velocity (or slowness) of each of which being an unknown parameter to be determined simultaneously, along with a and b. No anisotropic effects are considered in our study. Depending on the ray density, the mantle cell size can be as small as a fraction of one degree in arc distance. The resulting matrix equation describing the Pn travel times is generally large and sparse, and in our case is solved using a pre-conditioned version of LSQR algorithm of Paige and Saunders [1982], known for its computational efficacy and economy of CPU memory requirement. We describe below several key parameters that we will mention later in the text.

- Damping: A set of Laplacian damping equations regularizes slowness variations in the solution. The slowness regularization is governed by a damping coefficient (weight) that controls the trade-off between small errors in slowness (high damping) and narrow resolution width (low damping) [e.g., Menke, 1984].

- Cell: It is the elementary square for which the velocity is defined, somewhat analogous to the term pixel in image processing. Cell size is chosen to be shorter than the resolvable length, estimated from trial inversions using known velocity models.

Our goal has been to predict the Pn travel time. To this end, we have developed the algorithm to model the crustal delays that, when combined with the uppermost-mantle model, would predict the surface-to-surface Pn travel time. On the basis of station and event delays the delay for arbitrary grid point (x, y) is evaluated according to the formula:

$$\text{delay}(x, y) = \sum [\text{delay}(x_i, y_i) \cdot N_i \cdot W_i] / \sum [N_i \cdot W_i].$$

The expression $\text{delay}(x_i, y_i)$ pertains to crust delay for station/event located at the point (x_i, y_i); N_i the number of observations for given station/event; W_i, the geometrical weight of $\text{delay}(x_i, y_i)$, is equal to $(1 + k \cdot r_i^2 / R^2)^{-1}$; k is an empirical coefficient; r_i the distance between points (x, y) and (x_i, y_i); and finally, R is the maximum search radius.

Search radius R defines the area of averaging and is chosen to be as small as possible but still large enough to provide sufficient data to make continuous surface for given data density. Coefficient k defines degree of influence of the distant data and is chosen in such a way that yields geometrical weight equal to 1/10 on the edge of the search radius (k=9).

By varying the mantle cell size and damping weight, we have obtained several combinations of mantle velocity model and crust delays - none including anisotropy - before picking one. Our trial cell size was fixed at 1.0, 0.5, or 0.25 degree in arc length and our damping weight at 200, 400, or 600. Our objective is to find a model with a good

balance between the velocity error and the resolution width. Given the rather desirable station/event configuration, a weight of 600 allows adequate description of stable velocity features in most places - even when the cell is fixed at 0.25-degree in dimension.

For the chosen Pn velocity model we considered four crust delay models (with a search radius of 2, 3, 4, or 5 degrees). For our data density, a 3-degree search radius represents the smallest one that still yields a continuous delay surface over the whole territory. For this search radius, the crustal delay for each node of the 1-degree by 1-degree grid is determined using a minimum of 40 observations. We find that the resulting delay grid can cover the entire region of interest without any gaps.

We show the Pn velocity deviations from the reference Pn velocity (8.0 km/s) and crust delay map in Figures 7 and 9, respectively. In Figure 7 the Pn velocity image is superimposed with the main fault systems [Yuan Xuecheng, 1996], tectonic plate boundaries [Project PLATES, 2001], and the map of volcanoes [Global Volcanism Program, 2000]. The crust delay map (Figure 9) is superimposed with a shaded topographic map [ETOPO5].

Figure 8 represents Pn velocity tomography based on ABCE phase picks [Hearn and Ni, 2003]. With the data sources and the selection criteria discussed earlier, our dataset, comprising of 200,000 Pn phase picks, is about five times as voluminous as that of Hearn and Ni [2003]. The larger data volume – and hence higher Pn ray density - contributes to enhanced spatial resolution. The long-wavelength features in these two studies are consistent, as expected.

As seen in Figure 7, the cratons to the north of the Altay and Kunlun fault systems, such as Tarim, Junggar, and Qaidam Basins, are well outlined, with a Pn velocity of 8.2 km/s or higher.

The Tibetan Pn velocity is seen decreasing from south to north: from 8.0 – 8.15 km/sec at 30^0 N to 7.9 – 8.0 km/sec at the southern flank of Kunlun fault. McNamara et al., [1997] and Hearn and Ni [2003] attribute the relatively low velocity in northern Tibet to the presence of an underlying Indian lithosphere. A recent 3-D tomographic study by Xu et al., [2003] finds that the low Pn velocity is likely due to mantle upwelling and expansion associated with small-scale convections beneath northern Tibet.

In eastern China the Pn velocity is low. It is also more homogeneous than the findings by Hearn and Ni [2003]. A low-velocity feature is present at the western edge of the Pacific and Philippine Sea Plates - along the chain of volcanoes. Our study supports the conclusion of Hearn and Ni [2003] that there exists a low-velocity zone to the northwest of Hainan Island, near the southern edge of Red River fault system.
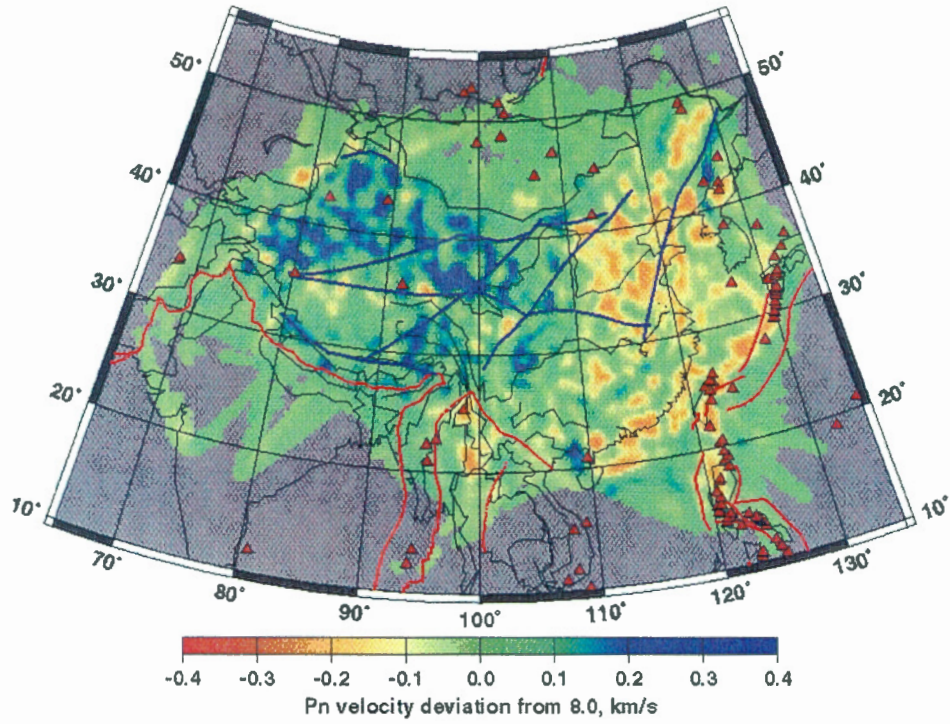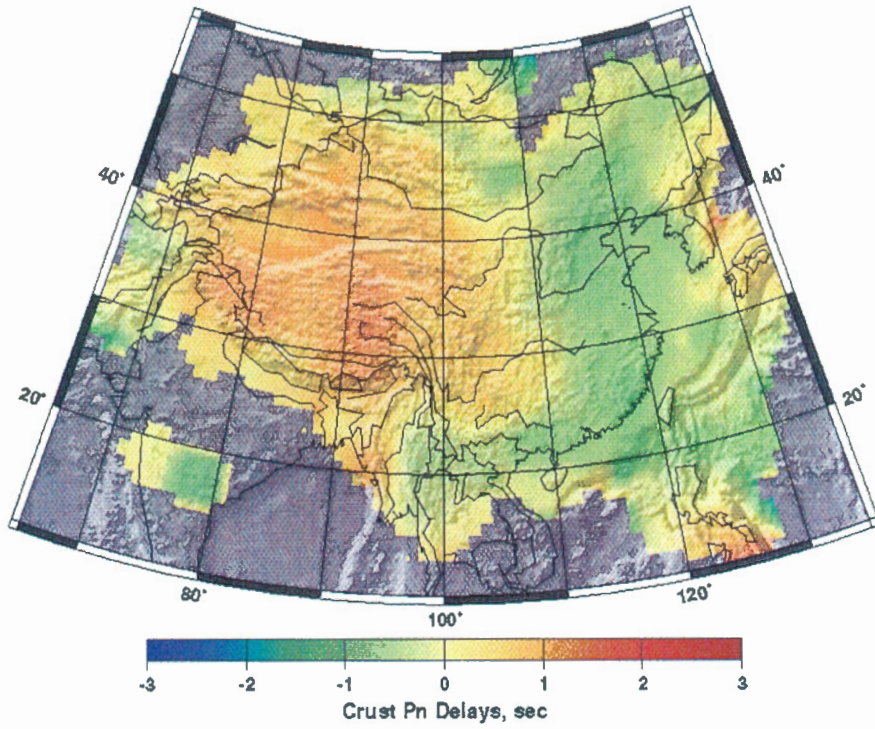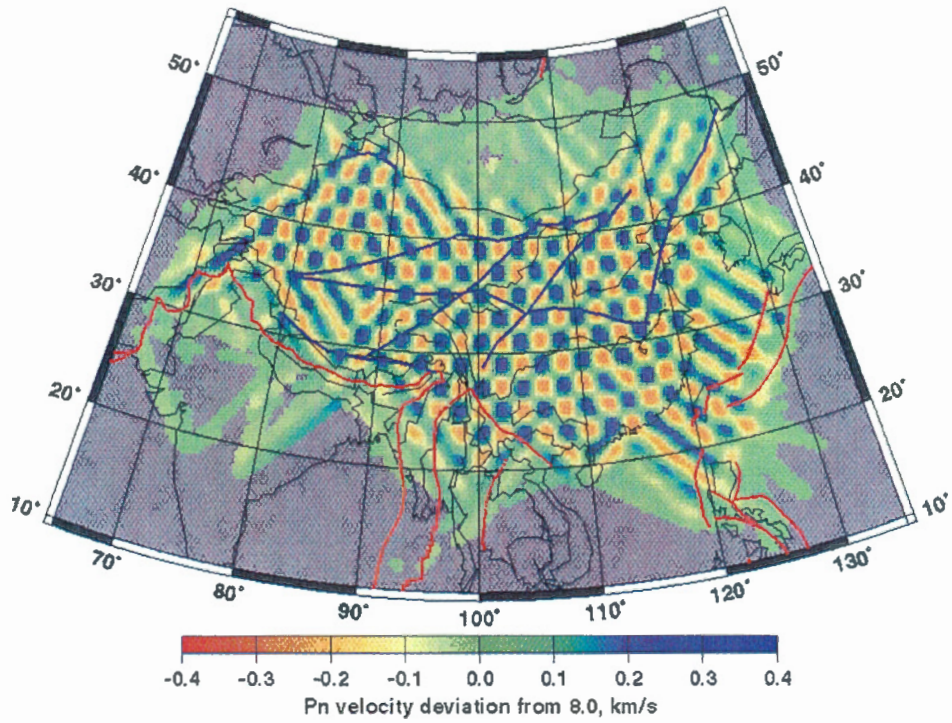
Figure 7. Pn velocity model (cell dimension: 0.25-deg.; damping weight: 600). Blue lines denote major fault systems: red line plate boundaries. Red triangles mark the sites of volcanoes.
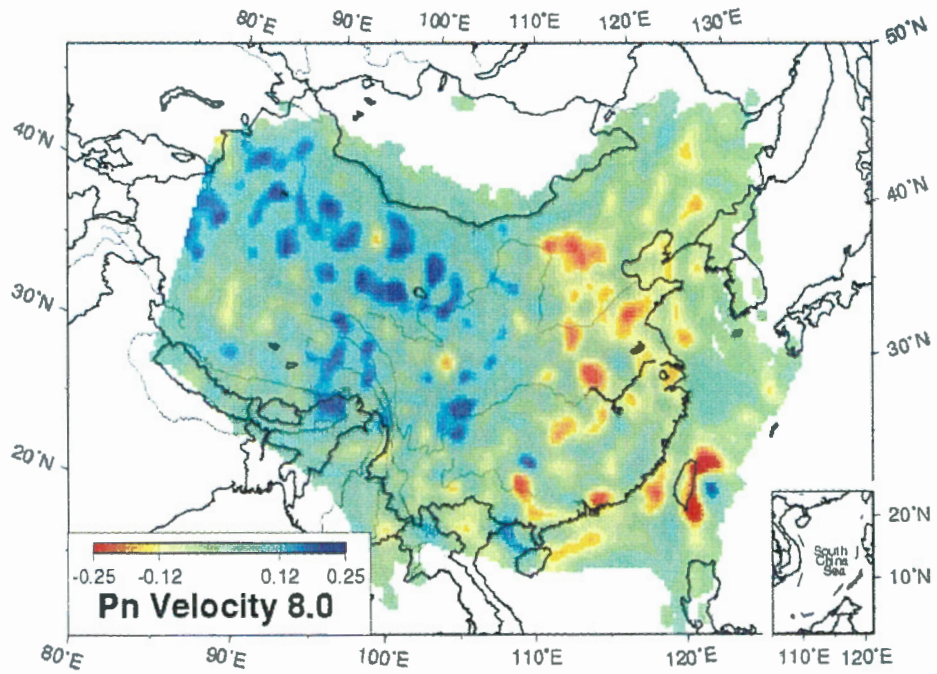
Figure 8. Pn tomography based on ABCE phase picks [Hearn and Ni, 2003]

Figure 9. Crust delay surface (3-deg. search radius) for Pn model shown in Fig. 7.

Figure 10. Pn velocities from the inversion of a test model featuring a sine function (amplitude= 0.25 km/s), a reference background velocity of 8.0 km/s, and $2^0 x 2^0$ cells.

We use the conventional checkerboard approach to estimate the resolving power of the Pn velocity model. Figure 10 shows the synthetic $2^0 \times 2^0$ grid. The checkerboard displays a good resolution of $2^0 \times 2^0$ for most parts of China. A notable exception is Tibetan Plateau where the ray coverage is the poorest (Figure 5).

4. SSSC AND MODELING ERRORS

We first process the reduced Pn travel-time data (Figure 3) to remove the outliers, as described earlier. We then fit a least-squares line to the processed data to obtain the reference Pn velocity and crustal delays from its slope and Y-intercept, respectively. Along any ray path, the mantle portion of the travel-time predicted by the reference Pn velocity is called reference Pn travel time.

Upon completing the development of the Pn model and crustal delay map, the actual calculations of the SSSC are rather straightforward. For any ray path, we first use the results of our Pn tomography to integrate travel-time deviations (from the reference Pn travel time). This cumulative travel-time deviation, when added to the reference Pn travel time and applicable crustal delays at an IMS station, produces the predicted Pn travel time along the ray path. The difference between this predicted value and the IASPEI-91 Pn travel time for the same epicentral distance is used to correct the latter.

Together with SSSCs we have evaluated modeling errors on the basis of our error estimations for Pn model and crustal delays. The inversion carried out using the entire dataset yields an *rms* error of 1.4 sec.

The crustal delay errors are determined according to the formula:

$$rms\_delay(x, y) = (\sum \{delay(x_i, y_i) - delay(x, y)\}^2 \cdot N_i \cdot W_i) / \sum[N_i \cdot W_i])^{0.5}.$$

where delay (x_i, y_i) are taken from the area around the point (x,y) within search radius R.

In a case when the both station (x_{sta}, y_{sta}) and the grid point (x_{grd}, y_{grd}) are covered by the model - and the epicentral distance does not exceed 14 degrees - the total modeling error is calculated as follows:

$$rms\_tot^2 = rms\_mantle^2 + rms\_delay(x_{sta}, y_{sta})^2 + rms\_delay(x_{grd}, y_{grd})^2.$$

When distance is beyond the range of interest (14 degrees) or if the grid point is outside the model, the modeling error is damped to the value of 4.0 (usual modeling errors for areas covered in this study are between 1.5 and 2.0 sec).

We have calculated SSSCs and modeling errors for all 16 IMS as well as for the 24 ABCE stations. The results are contained in the enclosed CD. Figures in Attachment 1 display their values.
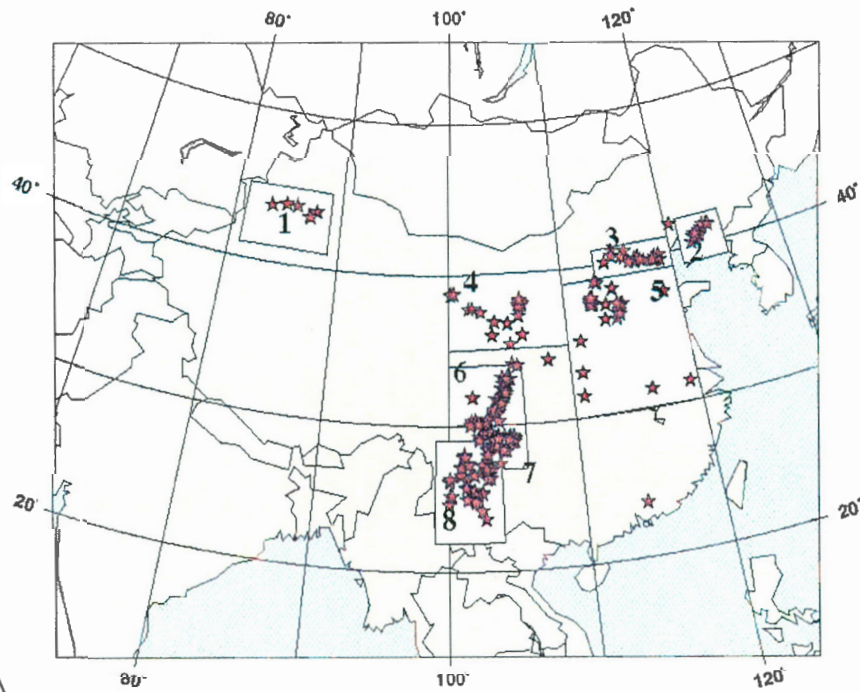
5. VALIDATION

Want of reliable ground truth events (GT0-GT5) constitutes a principal difficulty in any validation test. We selected 278 GT5 events, all of which are cross-referenced in the ABCE list on the basis of *sgap* criteria.

Unlike the Canadian case study, here we use only Pn phases for relocation. As well, we do not limit ourselves to IMS stations. Note that for data independence the phase information on these 278 GT5 events was deleted from the dataset actually used to produce Pn velocity model and SSSCs.

For relocation tests, we:
- Use code LocSAT, release 1.1, 2000;
- Fix event depths according to the AR/ABCE estimates;
- Use IASPEI-91 Pn as default travel-time (TT) tables;
- Compare epicentral locations derived with SSSCs and without;
- Require four or more stations, with a maximum azimuthal gap of less than 225^0.

Station affiliation with IMS is, however, not a requirement here. Figure 11 displays GT5 event locations; Figure 12 the relocation results. Attachment 2 contains information on epicentral location maps for regions marked in the Figure 11.

Figure 12. GT5 events used in validation test
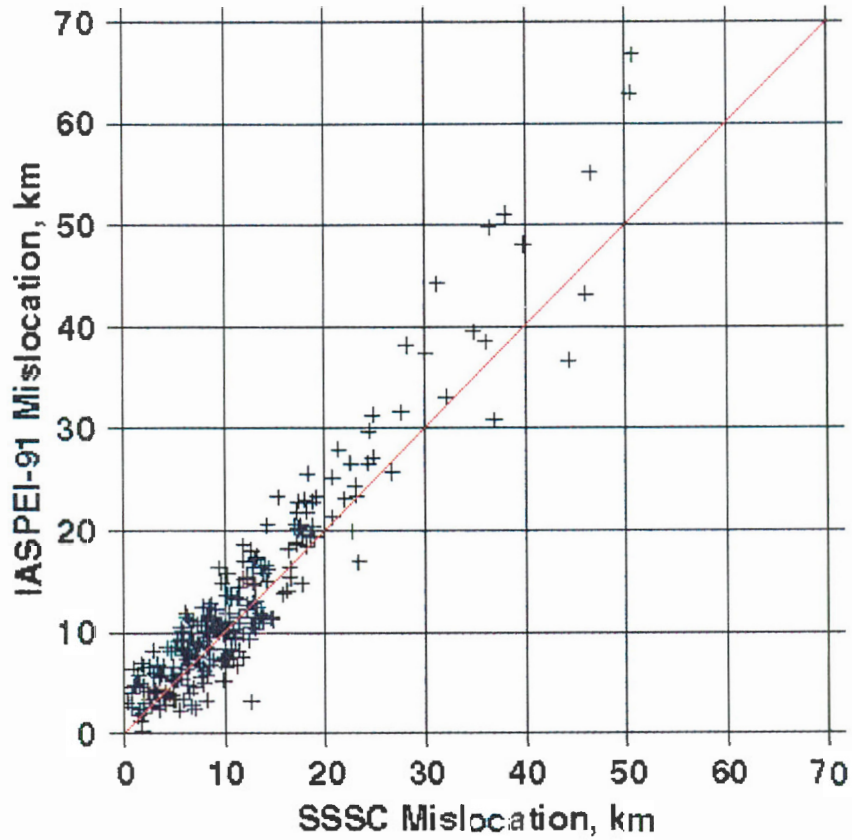
Figure 13. SSSC vs. IASPEI-91 mislocation for 278 GT5 events in China

As in the Canadian case study, we calculate the square root of the sum of squares of all SSSC and IASPEI-91 mislocations as a metric of location improvement. We use normalized mislocation as a metric of error ellipse coverage. The table below shows the results. Part A of our report contains the definitions of these metrics.

Location solution	Square root of sum of squares for mislocations, km	Normalized mislocation
SSSC	335	0.70
IASPEI	387	0.65

Finally, we tabulate the validation metrics in the table below.

Dataset characteristics

Number of events:	278
Average number of Pn phases per event	11
Average number of Pn phases within 14^0 from epicenter per event	7

Validation results

Percentage of events moving closer to GT5 event locations:	73%
Average improvement:	4.1km
Median improvement:	3.2 km
Percentage of events moving away from GT5:	27%
Average deterioration:	1.9km
Median deterioration:	1.3 km
Average 90% ellipse area for IASPEI-91:	1792 km^2
Median 90% ellipse area for IASPEI-91:	1415 km^2
Percentage of events covered by 90% error ellipse for IASPEI-91:	91%
Average 90% ellipse area for SSSC:	1367 km^2
Median 90% ellipse area for SSSC:	1107 km^2
Percentage of events covered by 90% error ellipse for SSSC:	89%
Average origin time difference between IASPEI-91 and GT5:	1.79 ±0.12 sec
Average origin time difference between SSSC and GT5:	-0.07 ±0.11 sec

The validation test poses a challenge. Some factors conspire to mask the usefulness of the SSSCs in epicentral location. For example:
- The majority of the GT5 events occurred in relatively homogeneous provinces. In such a case, the locations obtained with or without the SSSCs can differ only slightly.
- Since the station network coverage is excellent (on average, 11 Pn phases/event, as compared with 3.6/event in Canada – see Part A), the locations obtained without SSSCs are already fairly accurate, leaving less room for further improvement. The superiority of the SSSCs can stand out more clearly when the monitoring stations are scarce.

From the tables above, the changes in epicenter locations are of the order of a few kilometers. An ideal validation test, it seems, should involve the use of GT2 events or better. The above notwithstanding, our test does indicate that application of SSSCs improves the location. Many metrics calculated for the Chinese case study bear

resemblance to those in the Canadian case study. Most notable is the reduction in the size of error ellipse. This is partly due to the difference in number of stations with applicable SSSCs: we have on average 7 for the Chinese case and 3 for the Canadian case. The other reason is lower modeling error here that defines the ellipse size. The median area of the corrected error ellipse is 1107 km^2, not far from the 1000 km^2 target. Recall that the corresponding figure in the Canadian case study is as large as 2750 km^2.

Lop Nor Relocation

We have obtained, from CMR database, 20 GT events from Lop Nor Test Site, in NW China. Of these, 15 have produced sufficient number of Pn phase picks for relocation. Figure 14 shows the stations covered by the applicable Pn model and crustal delays. Only these are used for the relocation. Figure 15 displays the IASPEI-91 and the SSSC solutions. Figure 16 shows the error ellipse coverage for the IASPEI-91 solutions while Figure 17 shows the corresponding coverage for the SSSC solutions.
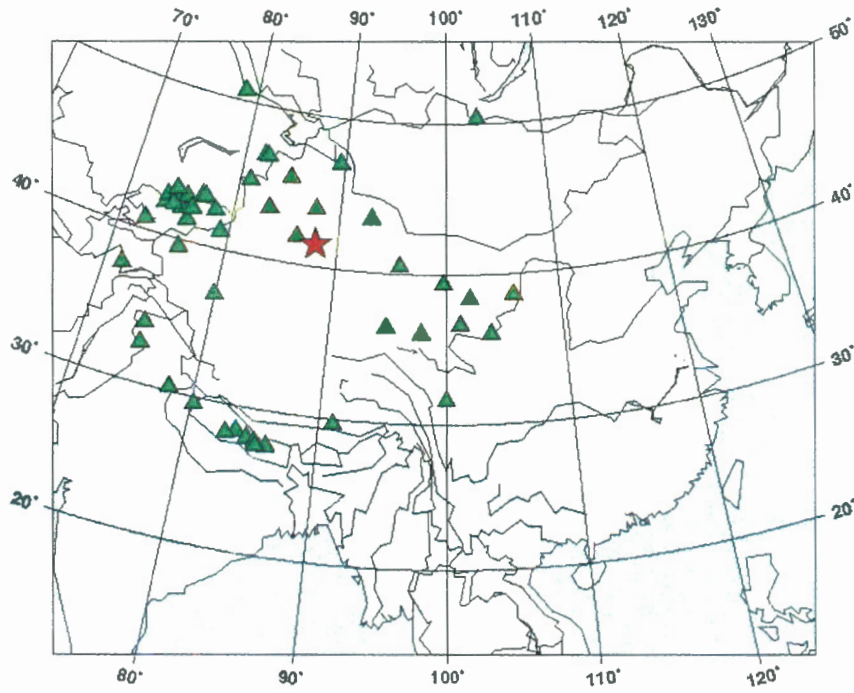
Figure 14. Stations recording Pn phases from Lop Nor Test Site
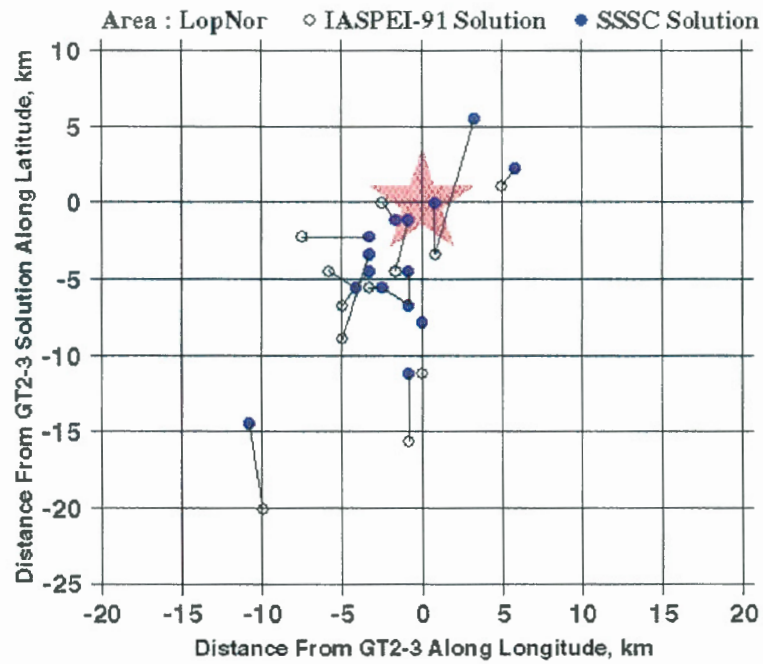
Figure 15. IASPEI-91 and SSSC solutions for 15 Lop Nor Nuclear Tests
(events are known with GT2, GT3 accuracy)
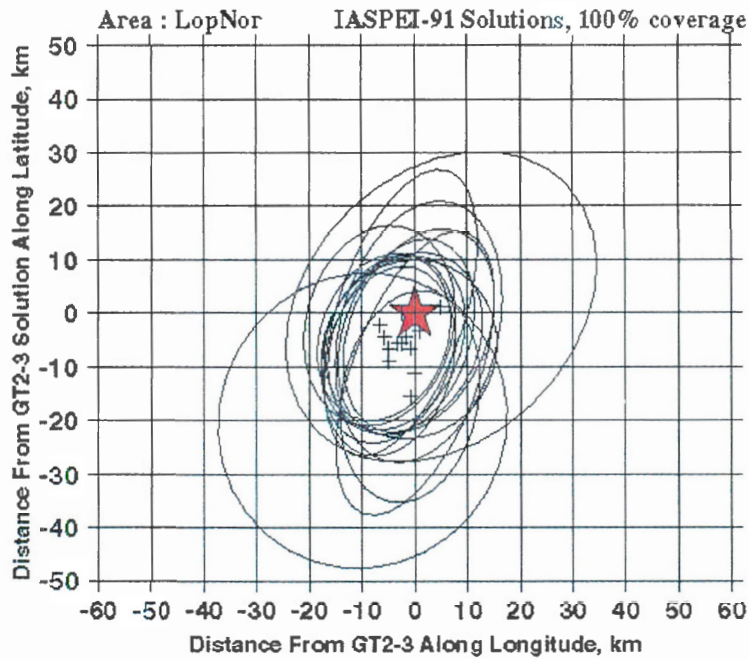
Figure 16. IASPEI-91 solutions and 90 % Error Ellipses for 15 Lop Nor Nuclear Tests;
100% of epicenters are covered by the ellipse
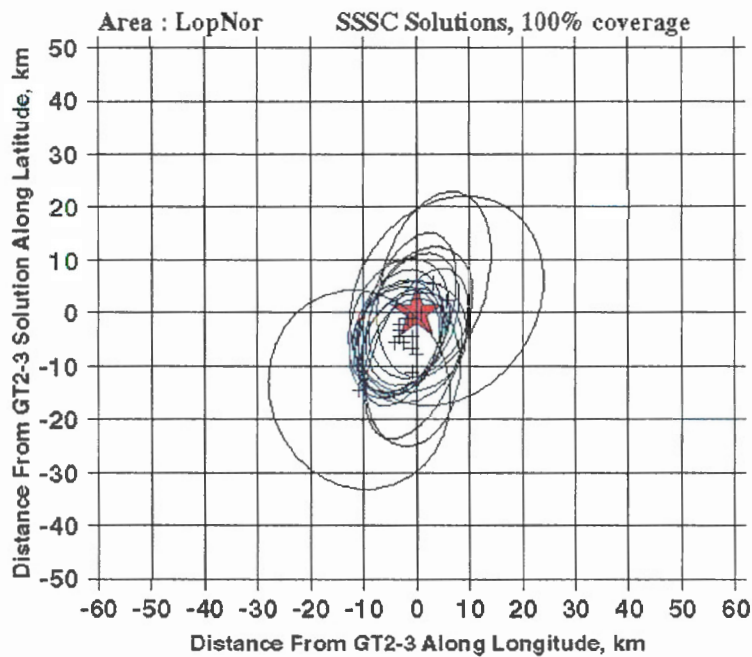
Figure 17. IASPEI-91 solutions and 90 % Error Ellipses for 15 Lop Nor Nuclear Tests;
100% of epicenters are covered by the ellipse

Tabulated below are some relevant results from our validation test.

Dataset characteristics

Number of events:	15
Average number of Pn phases per event	21
Average number of Pn phases within 14^0 from epicenter per event	21

Validation results

Median mislocation for IASPEI-91	7.0 km
Median mislocation for SSSC	5.5 km
Percentage of events moving closer to GT5:	80%
Median improvement	2.6 km
Percentage of events moving away from GT5:	20%
Median deterioration:	1.5 km
Median 90% ellipse area for IASPEI-91:	809 km^2
Percentage of events covered by 90% error ellipse for IASPEI-91:	100%
Median 90% ellipse area for SSSC:	432 km^2
Percentage of events covered by 90% error ellipse for SSSC:	100%
Average origin time difference between IASPEI-91 and GT5:	-0.16 ±0.12 sec
Average origin time difference between SSSC and GT5:	-2.27 ±0.10 sec

6. SUMMARY

The results of Part B have demonstrated the effectiveness of our method in improving the location accuracy for Eastern Asia case study. Geotectonic structures of the region are both interesting and complicated, with a thicker-than-normal crust overlaying a faster topmost mantle in Western China and a thinner crust overlaying a low-velocity mantle in much of eastern China. Pn tomography resolves well these crust/mantle features.

This study further develops our method for regional Pn travel-time calibration. We have shown how to solve the forward kinematic problem using modern Pn tomography. Whereas the Canadian case study uses a predefined crust model, here our Pn tomographic inversion determines simultaneously the crustal delays the mantle model. The results correlate well with known tectonic features of the Eastern Asia. We demonstrate their deployment produces corrections that improve epicentral location. Future improvement may come from the use of 3-D raytracer (distance up to 20^0). A 3-D tomographic model is currently being developed by us to facilitate the realization of such a possibility.

Acknowledgements

References

Bondar, I., S.C. Myers, E.R. Engdahl, E.A. Bergman (2002)
Epicenter Accuracy Based on Seismic Network Criteria. Submitted to
Geophysical Journal International

ETOPO5
5-min Gridded Topography Map of the World, National Geophysical Data Center,
National Oceanic and Atmospheric Administration, Global Relief Data and
Images, http://www.ngdc.noaa.gov/mgg/global/global.html

Global Volcanism Program (2000)
Smithsonian National Museum of Natural History, Global Volcanism Program,
Volcanoes of the World: On-Line Summaries, http://www.volcano.si.edu/world

Hearn, T.M. (1996)
Anisotropic Pn tomography in the western United States, J. Geophys. Res.,
101, B4, 8,403-8,414

Hearn, T.M. (1999), Uppermost mantle velocities and anisotropy beneath Europe,
J. Geophys. Res., 104, B7, 15,123-15,139

Hearn, T.M. and J.F. Ni (2003)
Uppermost mantle velocities beneath China and surrounding regions, J. Geophys.
Res., (submitted).

McNamara D.E., W.R. Walter, T.J. Owens, C.J. Ammon (1997)
Upper mantle velocity structure beneath the Tibetan Plateau from Pn travel time
tomography, J. Geophysical Research, 102, 493-505

Menke, W. (1984)
Sieve analysis as tomography, J. Sed. Petr., 54, 1358-1365.

Paige, C.C., and M.A. Saunders (1982a)
LSQR: An algorithm for sparse linear equations and sparse linear systems, ACM
Trans. Math. Software, 8, 43-71

Paige, C.C., and M.A. Saunders (1982b)
Algorithm 583 LSQR: Sparse linear equations and least square problems, ACM
Trans. Math. Software, 8, 195-209

Project PLATES (2001)
The University of Texas at Austin, Institute for Geophysics, The PLATES project,
http://www.ig.utexas.edu/research/projects/plates/0.htm

Wessel, P., W.H.F. Smith (1991)
  Free software helps map and display data, EOS Trans., AGU, 72, 441, 445-446
  http://imina.soest.hawaii.edu/gmt/

Xu, Y., F. Liu, J. Liu, and H. Chen (2003)
  Crust and upper mantle structure beneath western China from P wave travel time
  tomography, J. Geophys. Res., 107, B10, ESE 4-1.

Yuan Xuecheng (Chief Compiler) (1996)
  Atlas of geophysics in China, China Geological Publishing House, Publication
  No. 201 of the International Lithosphere Program

Appendix 1.
Source Specific Station Corrections and modeling errors for IMS stations

EVN

SSSC, s

Modeling Error, s

HAI

SSSC, s

Modeling Error, s

JAVM

SSSC, s

Modeling Error, s

KMI

SSSC, s

Modeling Error, s

KSRS

LZH

MAK

PPPK

SSE

URG

USK
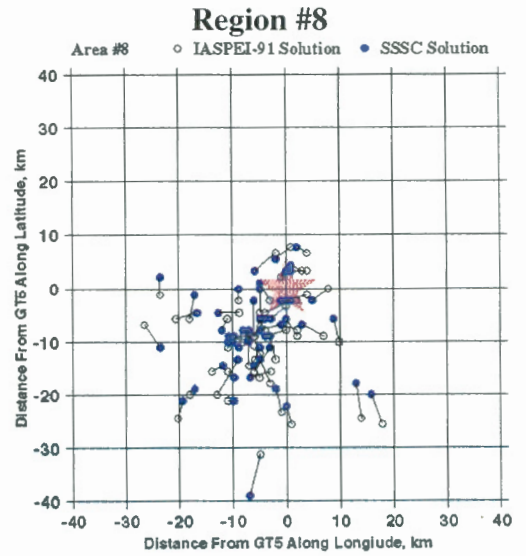
XAN

SSSC, s

Modeling Error, s
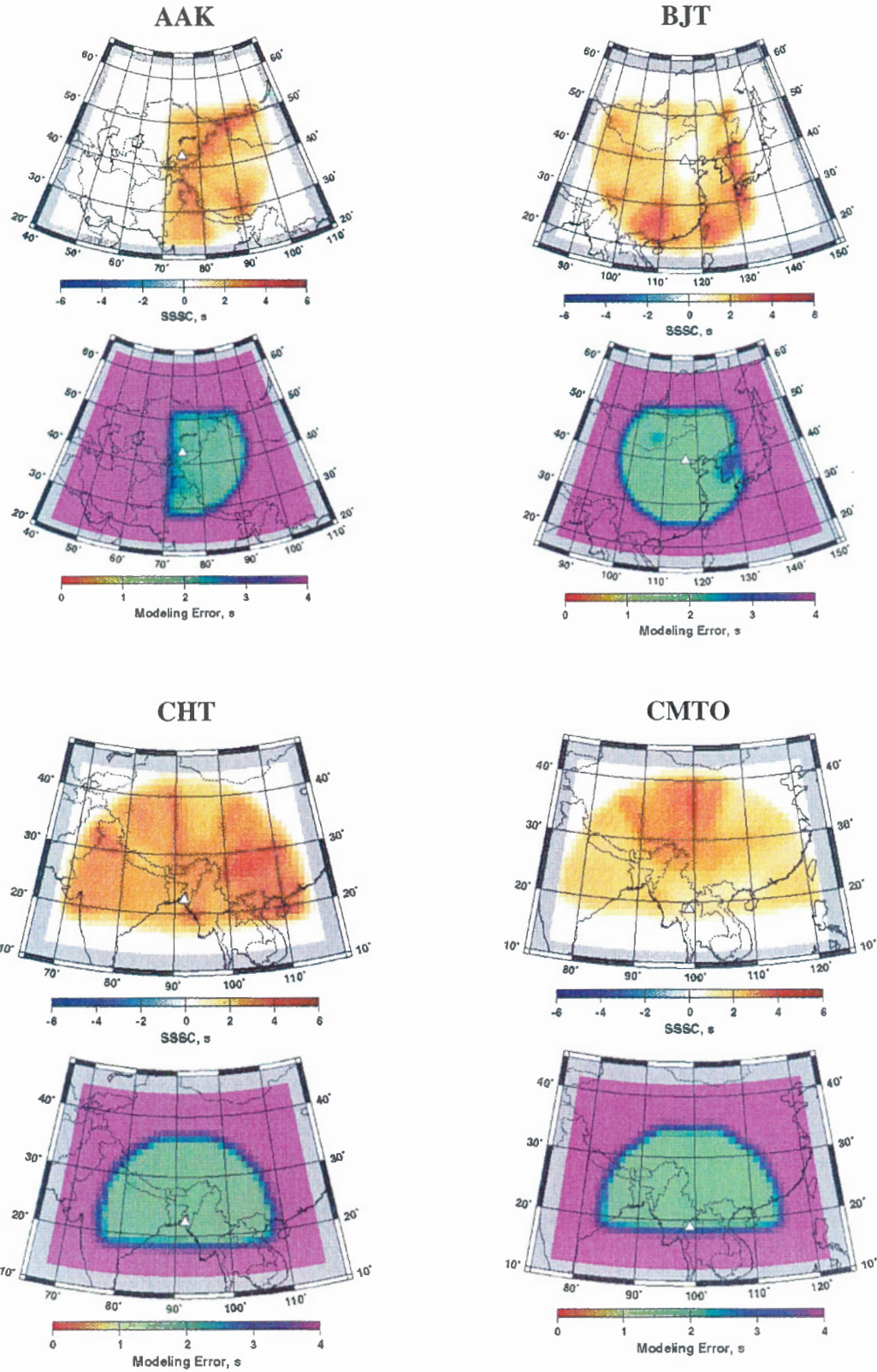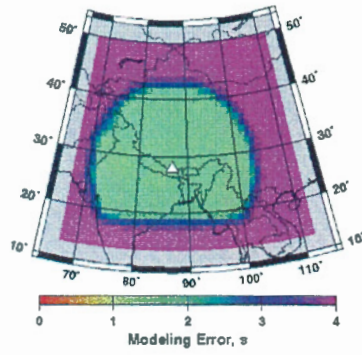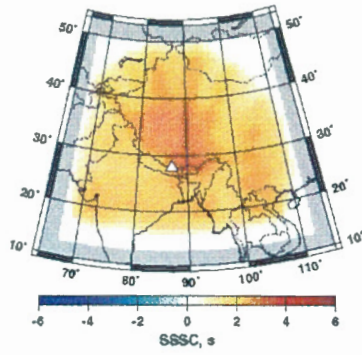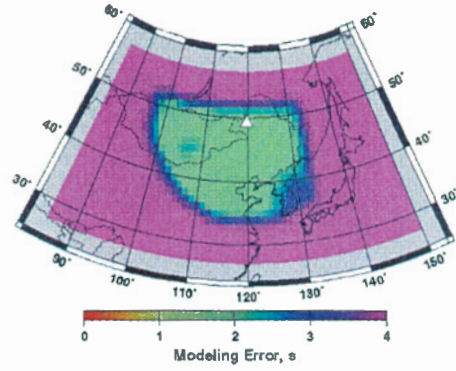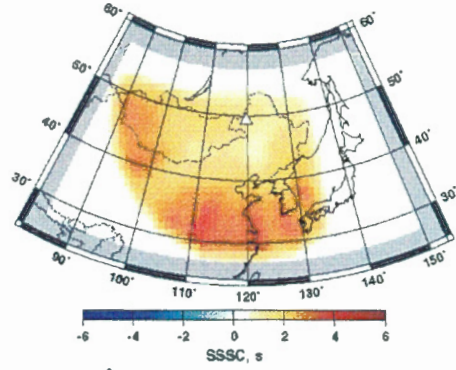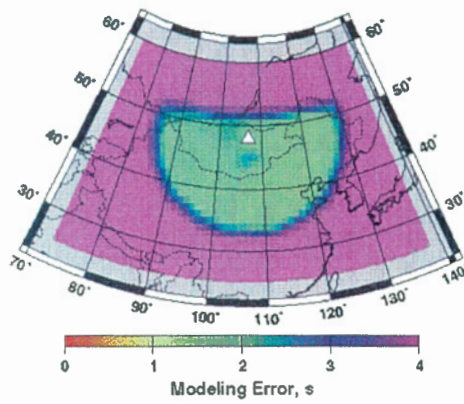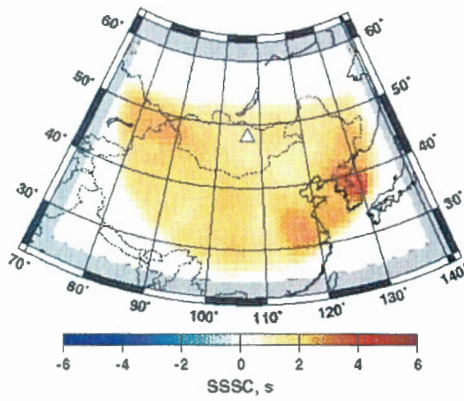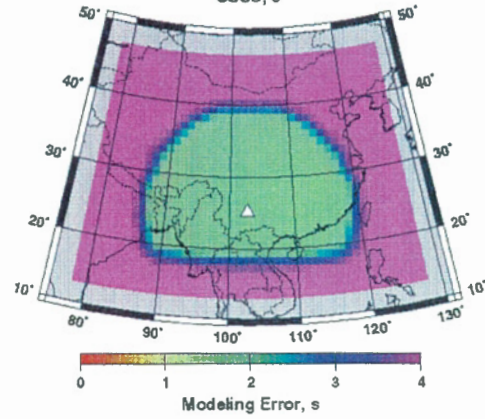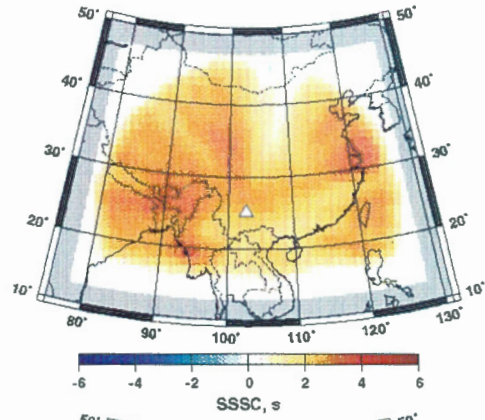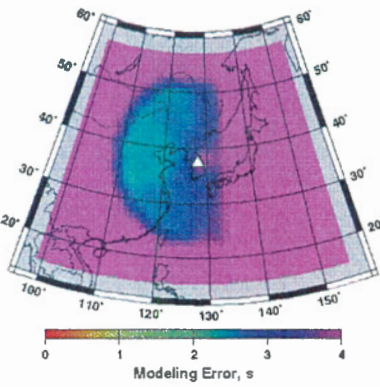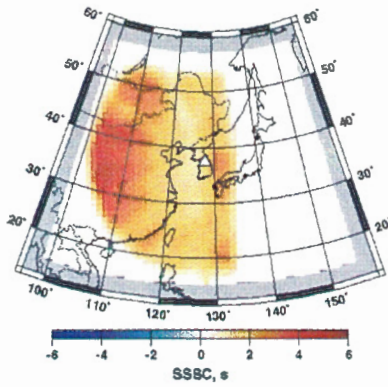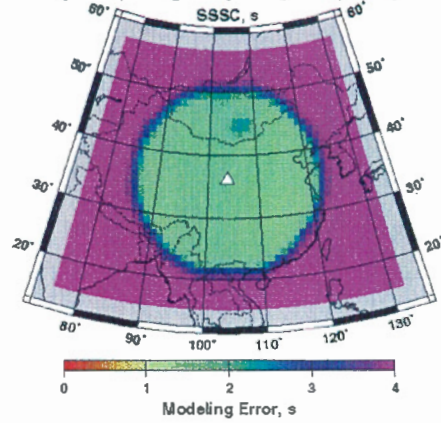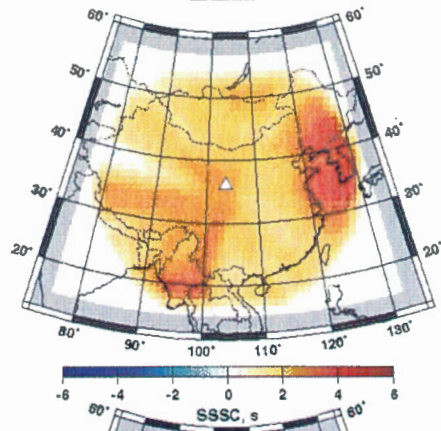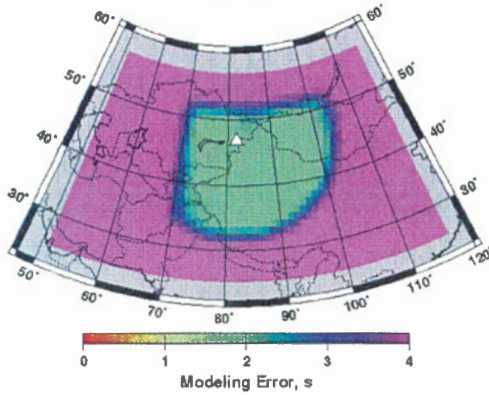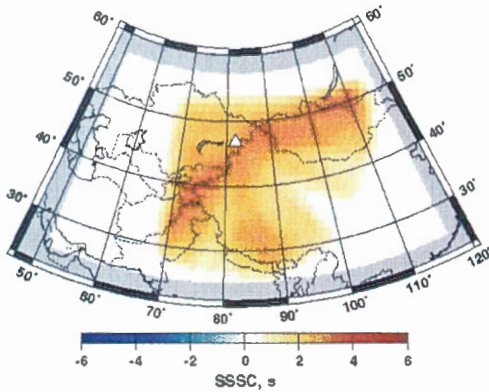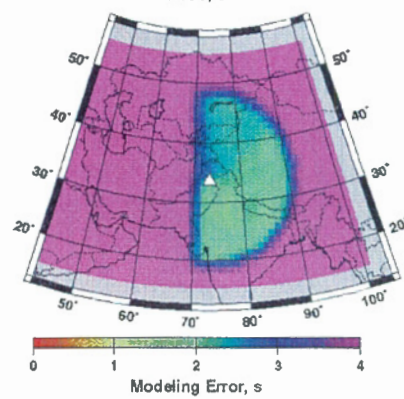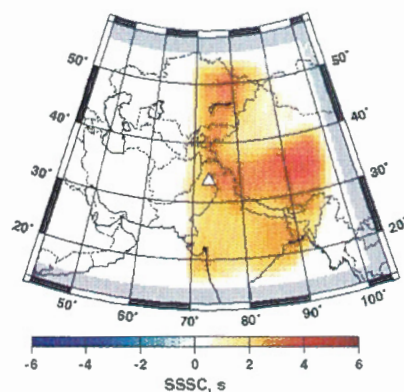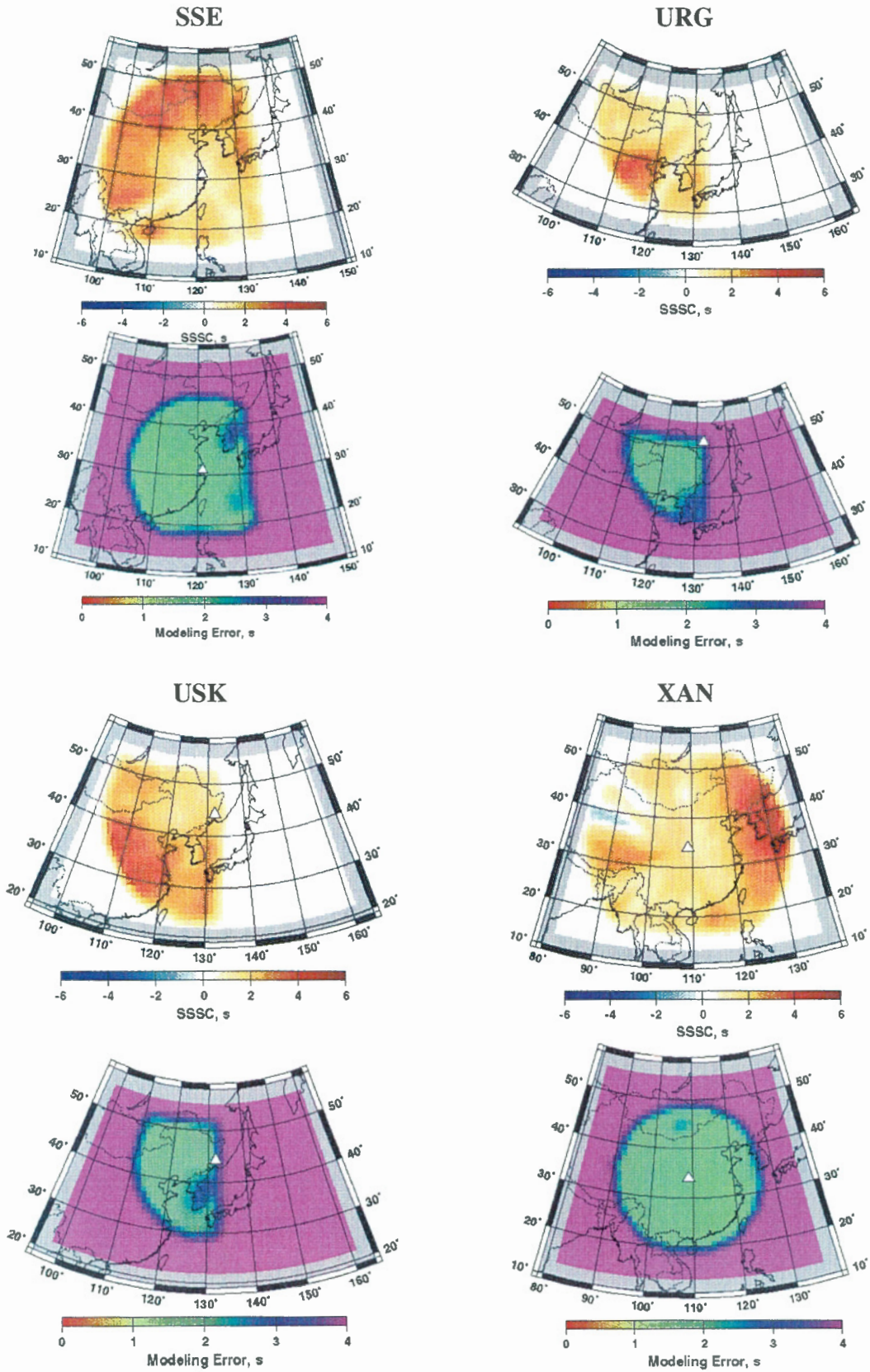
Appendix 2.
AR event relocation using SSSCs (Number of region corresponds to Figure 12 of the report)

Region #1

Region #2

Region #3

Region #4

Region #5

Region #6

Region #7

Region #8
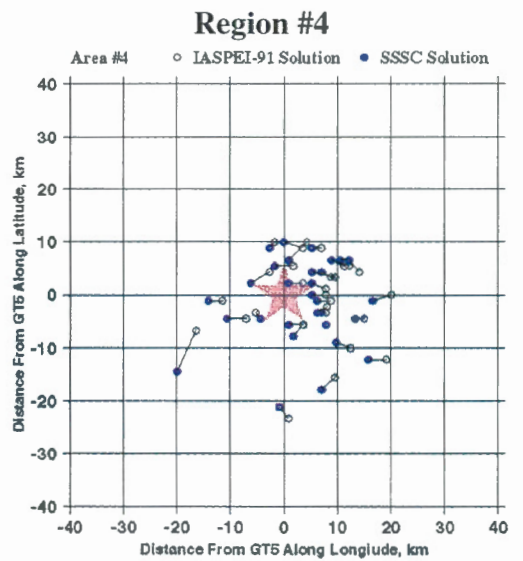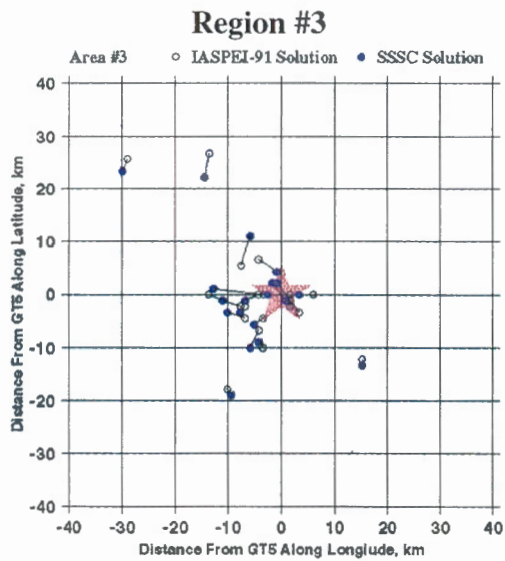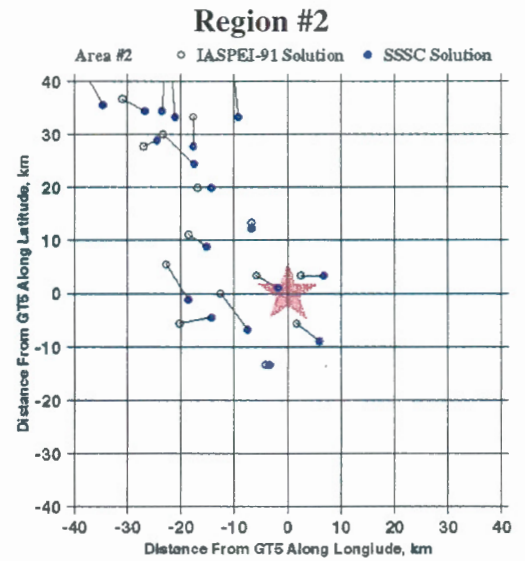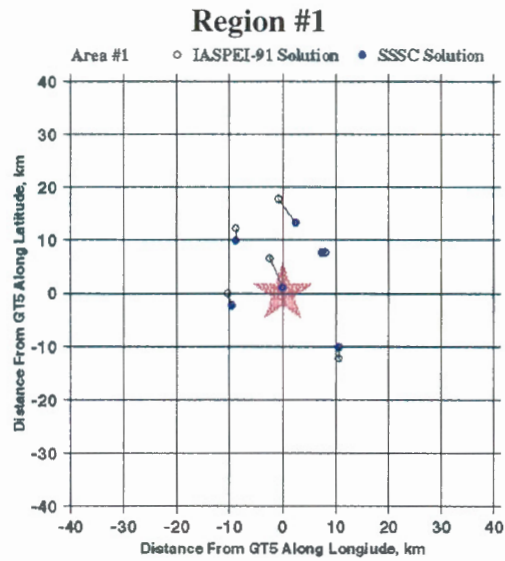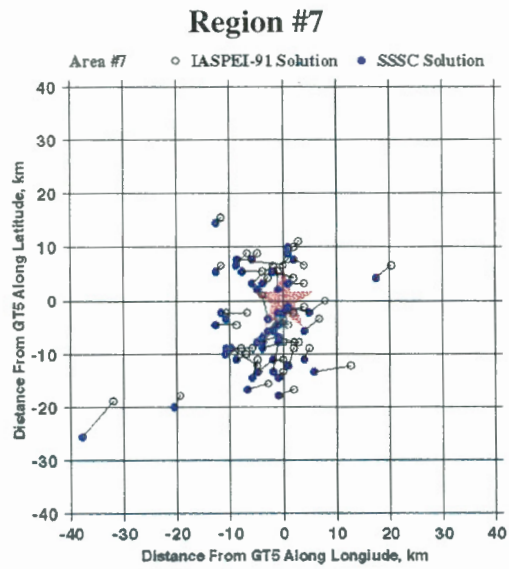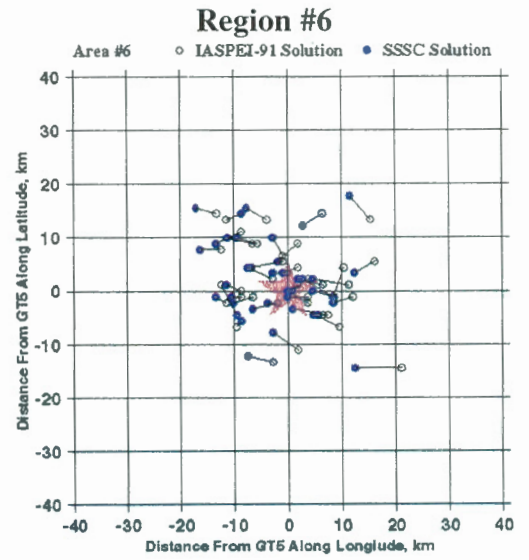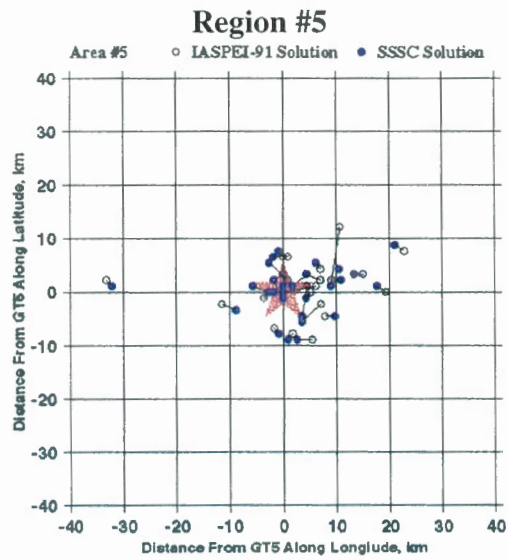
Appendix 3. Files on accompanying CD.

Item	Description	Format	File name
1. Pn tomographic and crust delay models for Eastern Asia			
Pn tomography model	Ctomo – produced Pn velocity tomography model for 0.25x0.25 degree grid	ASCII	B/model/dpn
Crust delay model	Crust delay model based on event and station delay for 1x1 degree grid	ASCII	B/model/delay
2. Pn SSSC and modeling error surfaces for IMS stations covered by the Pn tomography model in Eastern Asia			
Pn SSSC and modeling error surfaces around 16 IMS and 24 ABCE stations	SSSCs inferred using mantle model and crust delay model	1. ASCII IDC-compliant files 2. 2. ASCII flat files 3. SSSC and modeling error surfaces maps	B/SSSC/IMS/tt. *.Pn.reg.china B/SSSC/IMS/*.sssc B/SSSC/IMS/*.ps B/SSSC/ABCE/TT. *.Pn.reg.china B/sssc/ABCE/*.sssc
3. Ground Truth Event Candidates for Eastern Asia			
ABCE GT5 events and relocation results	278 events satisfying GT5 sgap criteria for local/near-regional zone, used for relocation	ASCII files	B/gt/abce_gt5
Lop Nor Nuclear Explosions data and relocation results	15 Lop Nor Nuclear Explosion data from CMR database: event, phase, station information; relocation results with and without SSSCs	ASCII files	B/gt/lopnor*